

ULRR

Oxygen evolution on metal#oxy#hydroxides: beneficial role of mixing Fe, Co, Ni explained via bifunctional edge/acceptor route

Item Type	Article
Authors	Vandichel, Matthias;Busch, Michael;Laasonen, Kari
Citation	ChemCatChem;12 (5), pp. 1436-1442
Publisher	John Wiley & Sons, Inc.
Download date	2026-06-14 20:02:43
Item License	https://creativecommons.org/licenses/by-nc-sa/1.0/
Link to Item	https://hdl.handle.net/10344/8726

Heterogeneous & Homogeneous & Bio- & Nano-

CHEMCATCHEM

CATALYSIS

Accepted Article

Title: Oxygen evolution on metal-oxy-hydroxides: beneficial role of mixing Fe, Co, Ni explained via bifunctional edge/acceptor route

Authors: Matthias Vandichel, Michael Busch, and Kari Laasonen

This manuscript has been accepted after peer review and appears as an Accepted Article online prior to editing, proofing, and formal publication of the final Version of Record (VoR). This work is currently citable by using the Digital Object Identifier (DOI) given below. The VoR will be published online in Early View as soon as possible and may be different to this Accepted Article as a result of editing. Readers should obtain the VoR from the journal website shown below when it is published to ensure accuracy of information. The authors are responsible for the content of this Accepted Article.

To be cited as: *ChemCatChem* 10.1002/cctc.201901951

Link to VoR: <http://dx.doi.org/10.1002/cctc.201901951>

Oxygen evolution on metal-oxy-hydroxides: beneficial role of mixing Fe, Co, Ni explained via bifunctional edge/acceptor route

Matthias Vandichel,^[a,b,c,*] Michael Busch,^[a] Kari Laasonen^[a]

Abstract: Oxygen evolution (OER) via mixed metal oxy hydroxides [M(O)(OH)] may take place on a large variety of possible active sites on the actual catalyst. A single site computational description assumes a 4-step electrochemical mechanism with coupled H⁺/e⁻ transfers between 4 intermediates (M^{*}, M-OH, M=O, M-OOH). We also consider bifunctional routes, in which an unstable M-OOH species converts via a proton shuttling pathway to a thermodynamically more favourable bare M^{*} site, O₂ and a hydrogenated acceptor site; the acceptor site takes up the proton forming a hydrogenated acceptor site after recombination with an electron from the catalyst material. Here, we combine pure metal γ -M(O)(OH) edge sites (M = Fe, Co, Ni) with as proton-acceptor sites different threefold coordinated oxygens on β -(M,M')(O)(OH) terraces (M,M' = Fe, Co, Ni). The acceptor sites on these terraces have of a M₂MO motif. Our combinatorial study results in a ranking of their bifunctional OER activity on a 3D-volcano plot. Via various bi- and tri-metallic oxy hydroxide combinations, we show that their excellent experimental OER activity results from bifunctionality and provide a roadmap to construct innovative low overpotential OER catalysts.

Introduction

Because of recent political choices made, sustainable energy demand is expected to increase substantially by 2050, which endorses us to constantly look for alternative renewable, cheap and environmentally friendly energy resources.^[1] Amongst other future technologies, hydrogen generation^[2] and the reduction of CO₂ to alcohols^[3] are expected to play an important role in this context. Splitting water into hydrogen and oxygen is one of many promising ways to effectively store excess wind, solar or other renewable energy during peak hours in the form of chemical bonds. These reactions are, however, unavoidably coupled with the generation of oxygen at the anode. While the reduction of water to hydrogen at the cathode is efficiently catalyzed by numerous cathode materials such as Pt^[4] or MoS₂,^[5] the oxidation of water to O₂ at the anode, presents the main bottleneck due to a significant overpotential that has to be paid.^[4c, 6] The oxygen evolution reaction (OER) or generation of O₂ at the anode represents therefore the main challenge in the

integration of an overall water splitting system^[7]. Currently, water oxidation is catalyzed by Dimensional Stable Anodes (DSAs) at an industrial scale.^[6a, 8] These consist of a mixture of scarce and expensive (Ru,Ir)O₂ mixed onto Ti.^[6a, 8] RuO₂ and IrO₂, when loaded onto Ti and Ir respectively, result in measured overpotentials of about 240 mV (RuO₂/Ti) and 270 mV (IrO₂/Ir) at 1mA/cm².^[9] However, to avoid the use of scarce metals, alternative catalysts based on Co, Cu, Mn, Fe, and Ni have been studied within the heterogeneous^[10] and homogeneous electrocatalysis communities.^[11] In alkaline solutions, the application of Co-, Ni-, Fe- and Mn-based transition metal oxides or hydroxides as OER electrocatalysts has been studied since 1950.^[10a, 12] Also the promotion effect of Fe on Ni(O)(OH) is known for more than three decades,^[12b, 12d] however, still actively investigated today.^[12a, 13] In alkaline solutions, bimetallic oxides, such as CoFeO_x and NiFeO_x, are low overpotential candidates.^[10a, 13a, 14] Moreover, Co-phosphate based catalysts (CoPi) have been promising self-healing catalysts that can stand proton-corrosion also at neutral pH.^[10, 15] The next generation OER catalysts may thus contain trimetallic oxides and phosphide-based pre-catalysts, which have been shown to yield low overpotentials of 200 mV at 10 mA/cm² for a mixed metal FeCoNiP ink impregnated on a glassy carbon electrode (GCE).^[16] This trimetallic FeCoNiP-based catalyst resulted in an even better OER behavior than the bimetallic analogues. Experimentally, the optimal Fe, Co, Ni trimetallic combination has been studied, with an optimal Ni:Fe ratio of 4 for the most active OER-catalyst.^[17] Furthermore, a mixed FeCoWO_x has also shown an astonishing low overpotential of 191 mV at 10 mA/cm² on a gold plated Ni-foam, and 223 mV on a standard GCE.^[18] It thus seems that these catalysts contain a high amount of highly active OER sites. Even for bimetallic oxides, such as NiFeO_x, the debate of the possible active sites is still ongoing with contradictory statements in computational literature onto the role of Ni and Fe.^[13a, 13c, 19] Within mixed Fe, Co and Ni-oxy hydroxides, there is a broad variety of active site possibilities, making it seemingly difficult to calculate the OER activity computationally.

Water oxidation proceeds via a complex mechanism which requires the subsequent removal of 4 protons and 4 electrons and the formation of an O-O bond.^[20] The mononuclear mechanism^[21] or single site mechanism proceeds through a series of four intermediates; **M^{*}**, **M-OH**, **M=O** and **M-OOH**. Of these species the **M=O** species has both the character of the **M=O** double bond and the **M-O•** radical, as verified within earlier studies.^[11a, 19b, 22] This mesomeric **M=O/M-O•** species is a challenging electronic structure and significant contributions from static correlation can be expected. Furthermore, such mesomeric structures have also been found for several transition metal complexes.^[23] Throughout this manuscript, we will refer to the **M=O/M-O•** species as **M=O**. Universal scaling relationships exist between the four intermediates **M^{*}**, **M-OH**, **M=O** and **M-OOH**, meaning that their energies are linearly dependent.^[6b, 21a] Due to these scaling relations, a constant difference of 3.2 eV needs, independent of the choice of catalyst, to be paid for the 2 e⁻/H⁺ oxidation of **M-OH** to **M-OOH**. This results in a minimal overpotential of 0.4 eV for this mononuclear mechanism.^[21] A short discussion on scaling relationships is presented in Supporting Information to provide additional background information to the reader.

[a] Dr. M. Vandichel, Dr. M. Busch, Prof. Dr. K. Laasonen
Department of chemistry and material science, School of chemical engineering, Aalto University
Kemistintie 1, 02150 Espoo, Finland

E-mail: matthias.vandichel@aalto.fi

[b] Dr. M. Vandichel
Department of Chemical Sciences and Bernal Institute,
Limerick University, Limerick, Ireland
E-mail: matthias.vandichel@ul.ie

[c] Dr. M. Vandichel
Department of applied physics, Aalto University,
Otakaari 1, 02150 Espoo, Finland

Supporting information for this article is given via a link at the end of the document. ((Please delete this text if not appropriate))

Besides the mononuclear mechanism, there are however alternative routes that might lead to lower overpotentials, such as the binuclear^[11o, 21d, 24] and the bifunctional^[21d, 25] mechanism. In the bi-nuclear mechanism, the formation of **M-OOH** is replaced by a recombination of 2 **M=O** surface species to form a μ -peroxo bridge which then desorbs through replacement of the **M-O** bonds by water. The bi-functional mechanism on the other hand is mechanically similar to the mononuclear mechanism in the sense that the O-O bond is formed through a nucleophilic attack of water or HO⁻ at a **M=O** oxo species. In contrast to the mono-nuclear path, however, the proton is transferred immediately to an adjacent H-acceptor unit. This step may either occur as a concerted 2H⁺/1e⁻ oxidation or render the **M-OOH** group so short-lived that it does not contribute significantly to the overall thermodynamic reaction profile.^[13a] These alternative reaction mechanisms in principle allow for water oxidation at negligible overpotential.^[10f, 13a, 21d, 25-26] This paper elaborates on the on-going debate for mixed metal oxy hydroxides by considering also the dual site or bifunctional mechanisms besides the standard single site or mononuclear mechanism. A detailed discussion about the generality of the bifunctional mechanism can be found in the perspective written by Busch.^[27]

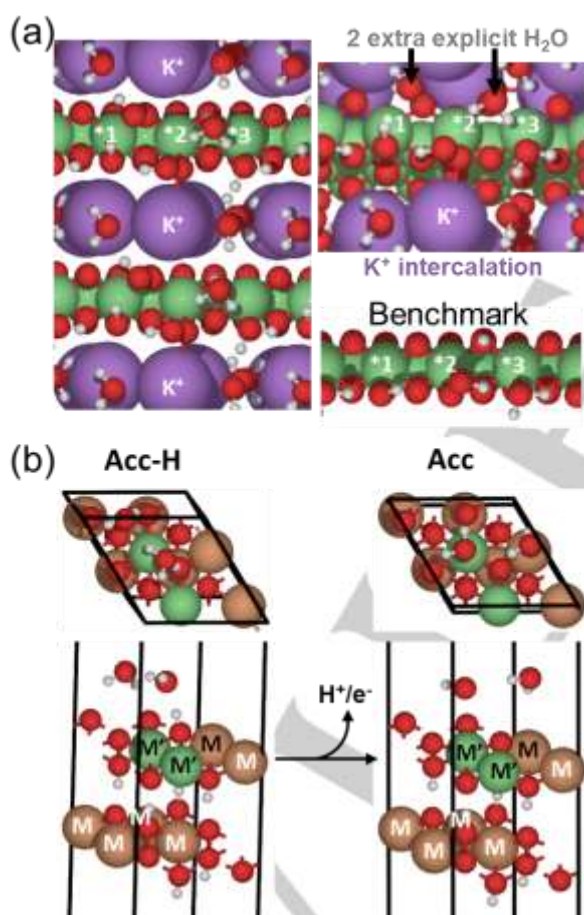


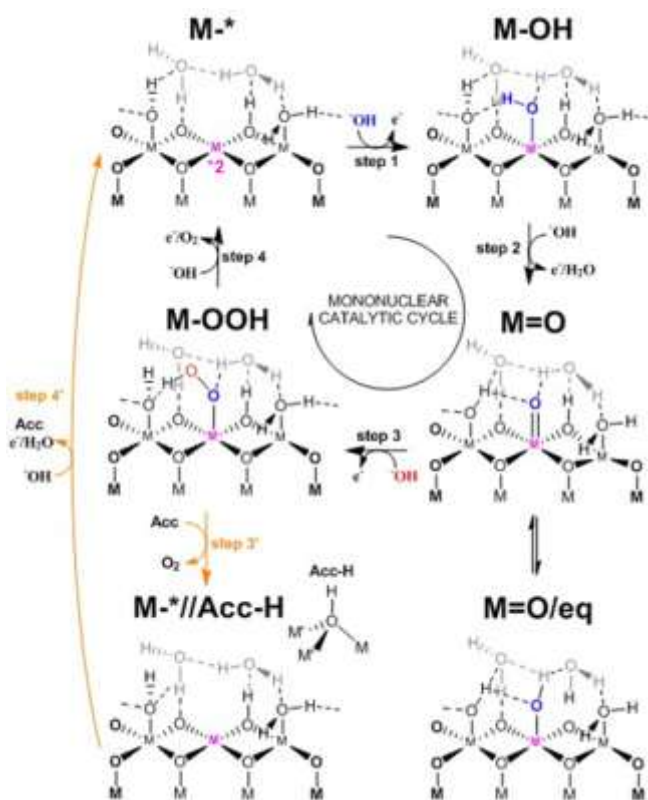
Figure 1. Model systems for (a) γ -M(O)(OH) edge model systems with explicit H₂O solvation versus benchmark model systems for edge sites, remark the 3 geometrically different active sites *1, *2 and *3; water and K⁺ intercalation [Bader charge K: +0.89 ± 0.01], in the benchmark system *1, *2 and *3 are more similar (b) hydrogenated acceptor and acceptor sites (Acc-H, Acc) of types M'M₂O and M'₂MO are available at the β -(M',M)(O)(OH)/M(O)(OH) terraces with explicit H₂O, denoted further as (M',M)/MOOH. Black lines represent unit cell box. Color codes: metals M, M' (green, brown), K (purple), O (red), H (white).

Here, we present an edge/acceptor screening process to study the thermodynamics of the oxygen evolution reaction under alkaline conditions according to the bifunctional route postulated recently for γ -(Fe,Ni)(O)(OH).^[13a] This screening study presents a 'best case' scenario based on DFT calculations of neutral reaction intermediates discussed above, and other factors such as the electrical conductivity and activation energy barriers are neglected. As models systems, we use existing edge model systems for γ -M(O)(OH) (Figure 1a) where hierarchical, alkali- and water intercalation as well as structural features of stacked nanosheets are present since these models are representative at alkaline OER-conditions.^[19b, 28]

Results and Discussion

The M(O)(OH) edges are combined with acceptor terraces, i.e. β -(M,M')(O)(OH)/(M)(O)(OH) or shorter (M,M')/(M)(O)(OH) (Figure 1b), which allows for the evaluation of different active edge site / acceptor combinations. Scheme 1 represents both the mononuclear and bifunctional pathway on an active γ -M(O)(OH) edge site. The intermediates on the γ -M(O)(OH) edge site in the mononuclear mechanism are **M***, **M-OH**, **M=O** and **M-OOH**. Due to the addition of two explicit water molecules (in gray, Scheme 1), the **M=O** species is in equilibrium with an **M=O/eq** species which is a mesomeric structure in which the oxo-species gets hydrogenated. Within the bifunctional mechanism an additional M'₂MO hydrogen acceptor site is present. This mechanism takes place if the critical **M-OOH** intermediate is unstable and converts back in a bare metal site **M***, O₂ and a hydrogenated acceptor site via an immediate H-transfer from the **M-OOH** species to an adjacent H-acceptor unit.^[25-26] In solvent, this reaction takes place via a proton shuttling mechanism, the acceptor site takes up the proton forming a hydrogenated acceptor site after recombination with an electron from the catalyst material. Thus, within the bifunctional mechanism, the M-OOH species can be seen as an unstable transitory intermediate.

Avoiding the universal scaling relations for OER catalysts is only possible if there are additional stabilizing factors (intercalation, van der Waals stabilization)^[29] or if there are alternative reaction routes.^[27] Within the bifunctional mechanism, the universal scaling relationship $\Delta G_{\text{M-OOH}} - \Delta G_{\text{M-OH}} = 3.2$ still holds, however, since **M-OOH** is an unstable transitory intermediate, we can replace its free energy by that of the subsequently formed more stable state; i.e. $\Delta G_{\text{O}_2} + \Delta G_{\text{Acc-H}} + \Delta G_{\text{M}^*} - \Delta G_{\text{Acc}} - \Delta G_{\text{M-OH}}$ and then the scaling relation does probably not hold any longer and can be avoided. To assess the likelihood of a bifunctional pathway, we define the descriptor DFBF (driving force bifunctional route). Because the global water splitting process, i.e. $2\text{H}_2\text{O} \rightarrow \text{O}_2 + 2\text{H}_2$, requires 4.92 eV and involves 4 proton/electron oxidation steps, an ideal catalyst would spend 1.23 eV per H⁺/e⁻ step. Therefore, the difference in free energy level of step 3 within a step plot with respect to an ideal OER catalyst is defined as the driving force for the bifunctional route (DFBF). DFBF is defined as $G^{\text{step1}} + G^{\text{step2}} + G^{\text{step3}} - 3.69$ eV, and can also be calculated from G^{step4} , $\text{DFBF} = 1.23 - G_4$. Thus if a mononuclear scaling relationship can be avoided, we can unravel the design criteria for optimal edge/acceptor combinations, which is highly interesting for the development of the next-generation bifunctional OER catalysts.



Scheme 1. Single site and dual site mechanism. Step 1, 2, 3 and 4 represent the electrochemical mononuclear OER mechanism under alkaline conditions on edge site *2 (purple) while step 1, 2, 3' and 4' represent the electrochemical bifunctional OER mechanism. The intermediate $M=O$ is in equilibrium with the $M=O/eq$. Hydrogenated acceptor sites (Acc-H) and acceptor sites (Acc) are required for the dual site mechanism.

Previously, the active phase of mixed (Ni,Fe)(O)(OH) systems was identified as γ -Ni(O)(OH)-like with a mixed formal oxidation state of +3.6 for the transition metal elements [19, 30] and representative potassium and water intercalated $M(O)(OH)$ systems have been used to describe electrocatalytic cycles computationally.[19b] Here, similar models for the pure metal edge sites are used [19b] while for the acceptor sites, layered oxy hydroxides are constructed (Figure 1a-b). Within the edge model systems, we investigated the mononuclear OER behavior of the three geometrically different active sites, indicated with *1, *2 and *3 (Figure 1a). For the acceptor sites considered in the bifunctional mechanism, variations of M' and M (Fe, Co, Ni) within β -(M',M)(O)(OH) unit cells. Besides three mono-metallic unit cells, there are six mixed metal unit cells, which have two types of three-fold coordinated acceptor sites (M'_2MO or $M_2M'O$). The system size of the acceptors is like these that were used in literature.[13a] However, here two parallel layers of metal oxy hydroxides are considered. It should be noted that solvation with two explicit water molecules within the acceptor systems is important. With only one H_2O or no H_2O , the behavior of the acceptor systems for the reaction displayed in Figure 1b, i.e. $Acc-H \rightarrow Acc + H^+/e^-$ is different. We refer to Table S7 for the acceptor behavior for the pure metal β -(M',M)/ $M(O)(OH)$ systems with less explicit solvation. Under alkaline pH, it is expected that the bifunctional mechanism will be more abundant than the mononuclear mechanism because of more available

proton acceptor sites, i.e. a lower proton coverage on the metal-oxy-hydroxides. In the following, we simplify the notations of the edge system γ - $M(O)(OH)$ and $M(O)(OH)$ to γ -MOOH and MOOH respectively.

For all γ -NiOOH-edge systems, the $M=O$ intermediate was also found to be thermodynamically unstable, equilibrating back to a significantly more stable intermediate $M=O/eq$ state (shown in Scheme 1). By allowing this more stable $M=O/eq$ the required potential for step 2 decreases. This creates an auspicious behavior in step 1 and 2 for the γ -NiOOH-edges (Figure 2c). However, it should be emphasized, that eventually during the formation of the $M-OOH$ intermediate from $M=O/eq$ and $\cdot OH$, there will be a higher transition state barrier. In the following, γ -MOOH-edges reacting via $M=O/eq$ will be referred to as γ -MOOH/eq edges.

The benchmark models are model systems without K^+ and water intercalation (Figure 1a). These yield overpotentials of 0.65 V (FeOOH edge), 0.35 V (CoOOH edge) and 0.58 V (NiOOH edge). The calculated overpotential for NiOOH on the benchmark edge is in good agreement with overpotentials from literature on similar edge systems; 0.52 V,[13c] and 0.61 V obtained using PBE+U and RPBE, respectively.[31] Only the overpotential value of Goddard and co-workers,[19b] i.e. 1.22 V (γ -NiOOH) is significantly different from these values because it was obtained with the hybrid functional B3PW91 instead of a regular GGA or GGA+U. However, for Fe-doped γ -NiOOH an overpotential of 0.45 V can be achieved, and further Co-, Rh-, or Ir-doping makes it possible to achieve even lower overpotentials of 0.27, 0.25 and 0.02 V, respectively.[28] For γ -FeOOH-edges, there is a reported overpotential of 0.45 V.[13a] Furthermore, to investigate the sensitivity of our BEEF-vdW results to the computational method used, we have performed benchmark calculations (Table S1) onto our γ -NiOOH-2* system using a regular GGA (PBE+U) functional as well as a hybrid functional with 25% exact exchange (HSE06). The overpotentials for the pathways proceeding via the $M=O/eq$ species are similar between PBE+U and BEEF-vdW, although the free energy differences between the steps vary (Table S1). At the HSE06-level, we obtain an overpotential of 1.09 eV, in line with the overpotential of 1.22 V obtained with a hybrid functional onto a system without two explicit waters.[19b] Such large overpotentials are a huge overestimation compared to experiments performed on pure NiOOH, with overpotentials of 0.4-0.5 V around $1mA.cm^{-2}$. [12g, 32] However, it is clear that both GGA+U and hybrid functionals are far off the experimental result. The charge localization in the single reference description with both GGA+U and hybrid functionals results in a destabilization of the $M=O$ species with respect to M^* .

Considering γ -edges, the most favorable mononuclear pathway has overpotentials of 0.95 V (γ -FeOOH-1*), 0.23 V (γ -CoOOH-2*) and 0.65 V (γ -NiOOH-1*), see Table S2, which also shows the large differences in OER performances among different active sites. These overpotentials are qualitatively in agreement with the benchmark edges. Although γ -NiOOH-1* has the lowest overpotential amongst all OER pathways studied on γ -NiOOH, the γ -NiOOH-2*/eq is selected for the further study, as this edge site can produce the most active edge/acceptor combinations according to a bifunctional reaction mechanism. Within Figure 2, the OER behavior of the three pure metal γ - $M(O)(OH)$ systems is represented in comparison with the ideal OER catalyst, where an H^+/e^- transfer would cost 1.23 eV. Compare the full black lines for γ -FeOOH-*3, γ -CoOOH-*2 and γ -NiOOH-*2/eq edges with the dashed lines (— —) representing ideal OER catalyst behavior.

To identify the most active edge/acceptor combinations, all edge acceptor combinations are tested for the bifunctional mechanism (Scheme 1). A schematic representation for both single site (mononuclear) and dual site (bifunctional) mechanism is available in Schemes S1-5, full screening results with Gibbs free energy differences for each of the four electrochemical steps are given in Tables S2-6. While the combination of edge acceptor sites results in various of possible oxygen evolution routes; there is a lot of possible routes that are equally good. A selection of such good results obtained from combining three different γ -M(O)(OH) edges with 3 different acceptors is presented in Table 1 and Figure 2. If the descriptor DFBF is larger than 0.0 eV or if the traditional G^{step3} is larger than 1.23 eV, there is a driving force for the bifunctional mechanism; this is the case pathway with the FeOOH-3* and NiOOH-2* edge, for which the standard mononuclear pathway has a very unstable M-OOH intermediate (see Table 1 and Figure 1). For the CoOOH-2* edge, the stability of the M-OOH intermediate is close to ideal, which is visible in a small value for DFBF (see Table 1). For the γ -FeOOH-3*, γ -CoOOH-2* and γ -NiOOH-2*/eq edges, we found bifunctional routes resulting in a significant lowering of the third step in a typical OER step plot (see intermitted dotted lines (· - · -), Figure 2). Figures 2a-c show the steps if the monometallic edges are combined with a favorable acceptor site with also other metals. In particular, we obtain overpotentials of 0.16 V (FeOOH-3*/(Ni,Co)/NiOOH-Ni₂CoO), 0.12 V (CoOOH-2*/(Fe,Ni)/FeOOH-Fe₂NiO and NiOOH-2*/eq/(Fe,Co)/FeOOH-Fe₂CoO edges) (Table 1 and Figure 2).

Interestingly, for some trimetallic edge/acceptor combinations, we find very low overpotentials (Figure 3). This emphasizes why trimetallic (Fe, Co, Ni) catalysts can outperform bimetallic OER catalysts [16]. However, within an OER catalyst only the most active sites and thus most active edge/acceptor combinations will eventually determine at which overpotential the catalytic cycle can light off, while the thermodynamic abundance of such active edge/acceptor combinations will determine the current density. In other words, only these edge/acceptor combinations that are close to the top of the bifunctional 3D volcano (Figure 3).

Consistent with previous studies, we find that in the best acceptor sites the presence of Fe is essential.^[32] Fe-containing acceptor sites are favored, as $G(\text{Acc-H}) - G(\text{Acc}) = G^{\text{step4}}$ in Table S3-6 is typically around 1.23 eV for most of these. Thus, pathways proceeding via the bifunctional mechanism containing such Fe-containing acceptor sites result automatically in a closer to ideal OER behavior, and thus lower overpotential. For example, the lowest overpotentials are found when combining the highly active γ -CoOOH and γ -NiOOH edges with mixed metal acceptors of high Fe-content (Table 1, Table S2-3). Ultimately, the bifunctional mechanism is most likely to happen at the γ -NiOOH-edges, as they display the highest driving force for bifunctional mechanism (DFBF, Table 1, S2-4). If a bifunctional mechanism is operative, then in particular the Fe₂NiO and Ni₂FeO acceptors of the (Fe,Ni)/FeOOH acceptor systems are amongst the acceptors that yield the lowest overpotentials (Table S3-4), around 0.12 V in case of a γ -NiOOH-2*/eq edge and around 0.17 V in case of a γ -FeOOH-3* edge. To guarantee a high abundance of the very active sites, new generations of materials based on γ - and β -mixed metal oxy hydroxides should contain all three metals from the iron triad (Fe, Co, Ni) with relatively high concentrations with Ni at the outer edge. The synthesis of such new morphologies of OER catalysts can be made by combining and modifying metal oxy

hydroxides or MOOH [33], or via the engineering porous coordination frameworks with a 2D-metal oxy hydroxide part [34].

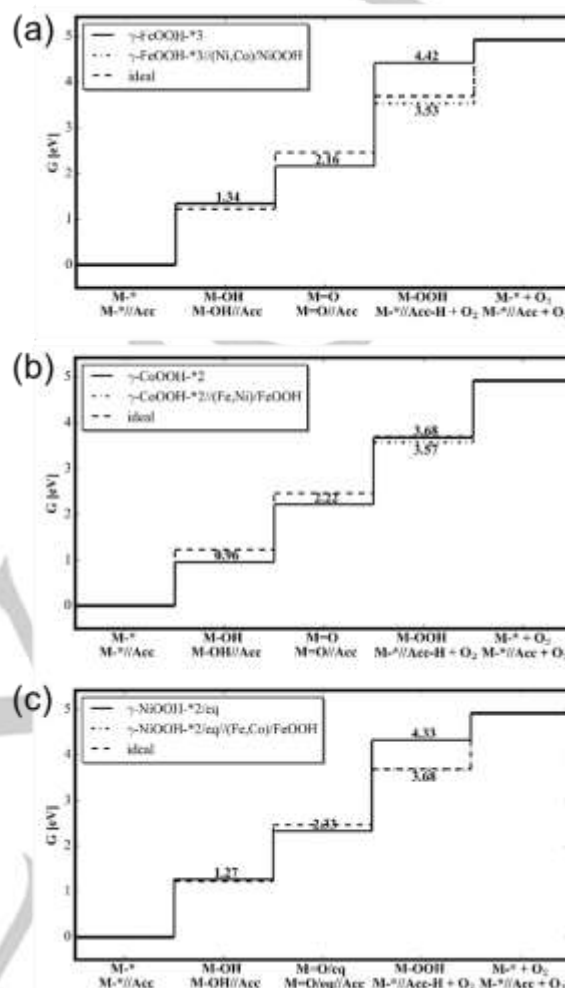


Figure 2. Beneficial behavior of M'M₂O acceptors site within β -(M,M')(O)(OH)/MOOH terraces on different edges; (a) γ -FeOOH-3*, (b) γ -CoOOH-2* and (c) γ -NiOOH-2*. Electrochemical step plots for the mononuclear and bifunctional pathways. The bifunctional pathways are also shown in Table 2 and Figure 3.

Table 1. Screening of different edge/acceptor combinations, with their respective minimum overpotential according to a bifunctional reaction mechanism η in eV. DFBF represent the driving force for the bifunctional edge/acceptor OER route.

η [V]	γ -M(O)(OH) EGDE	β -(M',M)/M(O)(OH) TERRACE	Z' ₂ ZO ACCEPTOR	DFBF [eV]
0.12	γ -NiOOH-2*/eq	(Fe,Co)/FeOOH	Fe ₂ CoO	0.64
0.12	γ -CoOOH-2*	(Fe,Ni)/FeOOH	Fe ₂ NiO	-0.01
0.12	γ -NiOOH-2*/eq	(Fe,Ni)/FeOOH	Fe ₂ NiO	0.64
0.16	γ -CoOOH-2*	(Ni,Co)/NiOOH	Ni ₂ CoO	-0.01
0.16	γ -FeOOH-3*	(Ni,Co)/NiOOH	Ni ₂ CoO	0.73
0.16	γ -NiOOH-2*/eq	(Ni,Co)/NiOOH	Ni ₂ CoO	0.64
0.18	γ -FeOOH-3*	(Fe,Ni)/FeOOH	Fe ₂ NiO	0.73
0.23	γ -CoOOH-2*	(Fe,Co)/FeOOH	Fe ₂ CoO	-0.01
0.29	γ -FeOOH-3*	(Fe,Co)/FeOOH	Fe ₂ CoO	0.73

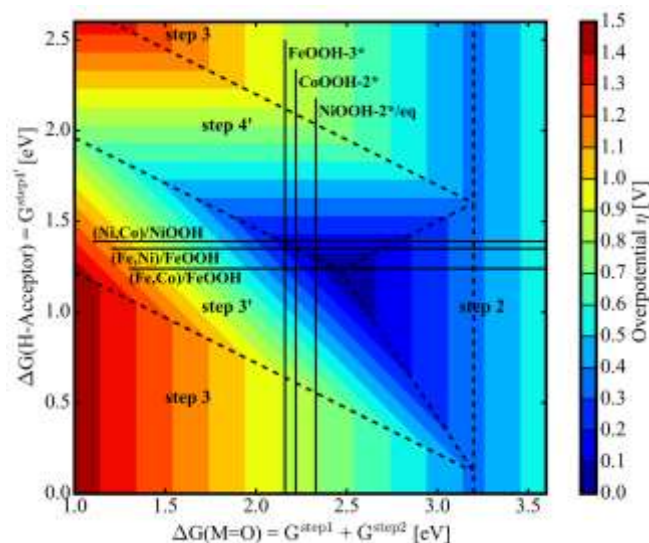


Figure 3. 3D volcano plot constructed from eq. 1, 2 and 4, with on the x-axis $\Delta G(\text{M}=\text{O}) = G^{\text{step1}} + G^{\text{step2}}$ [or $G(\text{M}=\text{O}) - G(\text{M}^*) - 0.5 \cdot G(\text{H}_2)$] for the active edge sites and on the y-axis $\Delta G(\text{Acc-H}) = E^{\text{step4}}$ [or $G(\text{M}_2(\text{OH})) - G(\text{M}_2(\text{O})) - 0.5 \cdot G(\text{H}_2)$]. Most active edge sites are combined with the best acceptor sites. Dotted lines separate regions with different rate determining steps. Crossing points between vertical lines (edges) and horizontal lines (acceptors) in the regions in which step 3', 4' and the triangular step 2 region are potential determining, and where the bifunctional mechanism leads to a lower overpotential pathway.

Conclusions

Summarizing, we have shown why mixed metal oxy hydroxides contain the best bifunctional edge/acceptor sites for OER, lowering the overpotential significantly compared to traditionally considered single site OER pathways. In a single site mechanism, an 'OH attack on a $\text{M}=\text{O}$ species of a γ -MOOH edge produces an $\text{M}-\text{OOH}$ species. If this species is unstable, there is a large driving force to react via the bifunctional pathway, whereby the proton transfers to a neighboring acceptor site, generating O_2 already in the third step. In case of mixed metal-oxo (M_2O) acceptor sites on β -MOOH sheets, there is a higher likelihood to have an optimal acceptor site, resulting in very low overpotentials. However, also other factors within mixed oxy hydroxides matter in OER performance assessments, such as the composition dependent conductivity, and reaction barriers which both increase the required overpotential. While reaction barriers can be computed,^[19b, 35] electronic conductivity is composition dependent and can be measured experimentally^[12g, 32].

Computational Section

To study the bifunctional mechanism for oxygen evolution reactions systematically, periodic DFT calculations are performed with the Vienna Ab Initio Simulation Package (VASP 5.4.4).^[36] Within transition metal catalysis, there are several examples where single reference calculations are not sufficient and multireference calculations are required.^[37] A similar multireference nature of the wavefunction has also been observed for molecular mononuclear OER catalysts.^[23] From this point of view, it is insufficient to correct only for the self-interaction error as done by using a DFT+U ansatz or hybrid

functionals. However, the M06L meta-GGA functional has been found to perform as well as many global hybrid functionals.^[23] In other words, M06 for mononuclear molecular OER catalysts^[23] and GGA functionals have been found to reproduce experimental overpotentials at solid-state OER catalysts accurately.^[13a, 38] Therefore, we opted for a semi-local gradient corrected (GGA) exchange-correlation functional in this study. The BEEF-vdW functional is employed to also account for van der Waals interactions for all reaction intermediates^[39]. The effect of water solvation is investigated by placing explicit water molecules around the intermediates. The one-electron Kohn-Sham orbitals were expanded in a plane wave basis set with a kinetic energy cut-off of 550 eV for all calculations. Furthermore, the projector augmented wave approximation (PAW) is used^[40]. A Gaussian smearing^[36a] of 0.1 eV is applied to improve convergence. Additionally, the convergence criterion for the electric self-consistent field (SCF) problem is set to 10^{-6} eV for cell optimizations. For Co and Ni, low spin states are assumed and for Fe high spin states. The total magnetization of each system is calculated according to the ligand field theory for octahedrally coordinated metals, in agreement with previous studies.^[10f, 11o, 13a, 19b] Free energy corrections are relative to the M^* state and water in liquid phase as determined by Man et al.^[21a] The edge and acceptor systems were structurally relaxed with $2 \times 2 \times 1$ and $4 \times 4 \times 1$ k-point grids respectively.

Acknowledgements

M.V. and K.L. acknowledges funding from Aalto University. The work was supported by the European Union's Horizon 2020 research and innovation program (CritCat Project, grant agreement no. 686053). We are grateful for the computing resources from CSC – IT Center for Scientific Computing.

Keywords: oxygen evolution reaction • Mixed metal oxy hydroxides • universal scaling relations • catalyst evaluation via 3D volcano • bifunctional route

References

- [1] a) S. Chu, A. Majumdar, *nature* **2012**, *488*, 294; b) C. Dette, M. R. Hurst, J. Deng, M. R. Nellist, S. W. Boettcher, *ACS Applied Materials & Interfaces* **2019**, *11*, 5590-5594.
- [2] T. Hisatomi, K. Domen, *Nature Catalysis* **2019**.
- [3] a) D. Kim, K. K. Sakimoto, D. Hong, P. Yang, *Angewandte Chemie International Edition* **2015**, *54*, 3259-3266; b) J. Qiao, Y. Liu, F. Hong, J. Zhang, *Chemical Society Reviews* **2014**, *43*, 631-675.
- [4] a) S. Trasatti, *J Electroanal Chem* **1972**, *39*, 163-8; b) J. Greeley, T. F. Jaramillo, J. Bonde, I. B. Chorkendorff, J. K. Norskov, *Nat Mater* **2006**, *5*, 909-913; c) M. Carmo, D. L. Fritz, J. Merge, D. Stolten, *Int J Hydrogen Energy* **2013**, *38*, 4901-4934.
- [5] T. F. Jaramillo, K. P. Jorgensen, J. Bonde, J. H. Nielsen, S. Horch, I. Chorkendorff, *Science* **2007**, *317*, 100-102.
- [6] a) H. Dau, C. Limberg, T. Reier, M. Risch, S. Roggan, P. Strasser, *Chemcatchem* **2010**, *2*, 724-761; b) M. T. M. Koper, *J Electroanal Chem* **2011**, *660*, 254-260.
- [7] a) N. S. Lewis, D. G. Nocera, *Proceedings of the National Academy of Sciences* **2006**, *103*, 15729-15735; b) J. Barber, *Chemical Society Reviews* **2009**, *38*, 185-196; c) T. Faunce, S. Styring, M. R. Wasielewski, G. W. Brudvig, A. W. Rutherford, J. Messinger, A. F. Lee, C. L. Hill, M. Fontecave, D. R. MacFarlane, *Energy & Environmental Science* **2013**, *6*, 1074-1076.
- [8] S. Trasatti, *Electrochim Acta* **2000**, *45*, 2377-2385.
- [9] N.-T. Suen, S.-F. Hung, Q. Quan, N. Zhang, Y.-J. Xu, H. M. Chen, *Chemical Society Reviews* **2017**, *46*, 337-365.

- [10] a) J. Suntovich, K. J. May, H. A. Gasteiger, J. B. Goodenough, Y. Shao-Horn, *Science* **2011**, *334*, 1383-1385; b) Z. Zhuang, W. Sheng, Y. Yan, *Advanced Materials* **2014**, *26*, 3950-3955; c) R. D. Smith, M. S. Prévot, R. D. Fagan, Z. Zhang, P. A. Sedach, M. K. J. Siu, S. Trudel, C. P. Berlinguette, *Science* **2013**, *340*, 60-63; d) J. Masa, W. Xia, I. Sinev, A. Zhao, Z. Sun, S. Grütze, P. Weide, M. Muhler, W. Schuhmann, *Angewandte Chemie International Edition* **2014**, *53*, 8508-8512; e) L.-A. Stern, L. Feng, F. Song, X. Hu, *Energy & Environmental Science* **2015**, *8*, 2347-2351; f) M. Busch, E. Ahlberg, I. Panas, *Catalysis Today* **2013**, *202*, 114-119; g) F. Song, X. L. Hu, *Nature Communications* **2014**, *5*; h) J. Masa, W. Xia, I. Sinev, A. Zhao, Z. Sun, S. Grütze, P. Weide, M. Muhler, W. Schuhmann, *Angewandte Chemie International Edition* **2014**, *53*, 8508-8512; i) Y. Surendranath, M. W. Kanan, D. G. Nocera, *J Am Chem Soc* **2010**, *132*, 16501-16509; j) D. González-Flores, I. Sánchez, I. Zaharieva, K. Klingan, J. Heidkamp, P. Chernev, P. W. Menezes, M. Driess, H. Dau, M. L. Montero, *Angewandte Chemie International Edition* **2015**, *54*, 2472-2476; k) J. Huang, J. Chen, T. Yao, J. He, S. Jiang, Z. Sun, Q. Liu, W. Cheng, F. Hu, Y. Jiang, Z. Pan, S. Wei, *Angewandte Chemie International Edition* **2015**, *54*, 8722-8727; l) M. M. Najafpour, T. Ehrenberg, M. Wiechen, P. Kurz, *Angewandte Chemie International Edition* **2010**, *49*, 2233-2237; m) M. S. El-Deab, M. I. Awad, A. M. Mohammad, T. Ohsaka, *Electrochemistry Communications* **2007**, *9*, 2082-2087; n) A. Ramírez, P. Hillebrand, D. Stellmach, M. M. May, P. Bogdanoff, S. Fiechter, *The Journal of Physical Chemistry C* **2014**, *118*, 14073-14081; o) F. Cheng, X. Feng, X. Chen, W. Lin, J. Rong, W. Yang, *Electrochimica Acta* **2017**, *251*, 336-343.
- [11] a) Y. Zhao, J. Lin, Y. Liu, B. Ma, Y. Ding, M. Chen, *Chemical Communications* **2015**, *51*, 17309-17312; b) D. Shevchenko, M. F. Anderlund, A. Thapper, S. Styring, *Energy & Environmental Science* **2011**, *4*, 1284-1287; c) D. Das, S. Pattanayak, K. K. Singh, B. Garai, S. Sen Gupta, *Chemical Communications* **2016**, *52*, 11787-11790; d) C. Lu, J. Du, X.-J. Su, M.-T. Zhang, X. Xu, T. J. Meyer, Z. Chen, *ACS Catalysis* **2015**, *6*, 77-83; e) S. M. Barnett, K. I. Goldberg, J. M. Mayer, *Nature chemistry* **2012**, *4*, 498-502; f) Z. Chen, T. J. Meyer, *Angewandte Chemie International Edition* **2013**, *52*, 700-703; g) M.-T. Zhang, Z. Chen, P. Kang, T. J. Meyer, *Journal of the American Chemical Society* **2013**, *135*, 2048-2051; h) W. C. Ellis, N. D. McDaniel, S. Bernhard, T. J. Collins, *Journal of the American Chemical Society* **2010**, *132*, 10990-10991; i) J. L. Fillol, Z. Codolà, I. Garcia-Bosch, L. Gómez, J. J. Pla, M. Costas, *Nature chemistry* **2011**, *3*, 807-813; j) C. Panda, J. Debgupta, D. D. Diaz, K. K. Singh, G. S. Sen, B. B. Dhar, *Journal of the American Chemical Society* **2014**, *136*, 12273-12282; k) D. Wang, G. Ghirlanda, J. P. Allen, *Journal of the American Chemical Society* **2014**, *136*, 10198-10201; l) L. Wang, L. Duan, R. B. Ambre, Q. Daniel, H. Chen, J. Sun, B. Das, A. Thapper, J. Uhlig, P. Dinér, *Journal of Catalysis* **2016**, *335*, 72-78; m) Y. Han, Y. Wu, W. Lai, R. Cao, *Inorganic Chemistry* **2015**, *54*, 5604-5613; n) J. Limburg, J. S. Vrettos, H. Y. Chen, J. C. de Paula, R. H. Crabtree, G. W. Brudvig, *Journal of the American Chemical Society* **2001**, *123*, 423-430; o) M. Busch, E. Ahlberg, I. Panas, *Phys Chem Chem Phys* **2011**, *13*, 15069-15076; p) H. A. Younus, N. Ahmad, A. H. Chughtai, M. Vandichel, M. Busch, K. Van Hecke, M. Yusubov, S. X. Song, F. Verpoort, *Chemosuschem* **2017**, *10*, 862-875.
- [12] a) H. Bode, K. Dehmelt, J. Witte, *Electrochimica Acta* **1966**, *11*, 1079-11071; b) D. A. Corrigan, *J. Electrochem. Soc.* **1987**, *134*, 377-384; c) S. E. S. El Wakkad, A. Hickling, *Transactions of the Faraday Society* **1950**, *46*, 820-824; d) G. Mlynarek, M. Paszkiewicz, A. Radniecka, *Journal of Applied Electrochemistry* **1984**, *14*, 145-149; e) M. Morita, C. Iwakura, H. Tamura, *Electrochimica Acta* **1977**, *22*, 325-328; f) J. W. Schultze, S. Mohr, M. M. Lohrengel, *Journal of Electroanalytical Chemistry and Interfacial Electrochemistry* **1983**, *154*, 57-68; g) L. Trotochaud, S. L. Young, J. K. Ranney, S. W. Boettcher, *J Am Chem Soc* **2014**, *136*, 6744-6753.
- [13] a) F. Song, M. M. Busch, B. Lassalle-Kaiser, C.-S. Hsu, E. Petkucheva, M. Bensimon, H. M. Chen, C. Corminboeuf, X. Hu, *ACS Central Science* **2019**; b) S. Klaus, M. W. Louie, L. Trotochaud, A. T. Bell, *The Journal of Physical Chemistry C* **2015**, *119*, 18303-18316; c) Y.-F. Li, A. Selloni, *ACS Catalysis* **2014**, *4*, 1148-1153.
- [14] a) M. Hamdani, R. N. Singh, P. Chartier, *Int. J. Electrochem. Sci.* **2010**, *5*, 556-577; b) M. D. Merrill, R. C. Dougherty, *The Journal of Physical Chemistry C* **2008**, *112*, 3655-3666.
- [15] M. W. Kanan, Y. Surendranath, D. G. Nocera, *Chemical Society Reviews* **2009**, *38*, 109-114.
- [16] J. Y. Xu, J. J. Li, D. H. Xiong, B. S. Zhang, Y. F. Liu, K. H. Wu, I. Amorim, W. Li, L. F. Liu, *Chem Sci* **2018**, *9*, 3470-3476.
- [17] R. D. L. Smith, M. S. Prévot, R. D. Fagan, S. Trudel, C. P. Berlinguette, *J Am Chem Soc* **2013**, *135*, 11580-11586.
- [18] B. Zhang, X. Zheng, O. Voznyy, R. Comin, M. Bajdich, M. García-Melchor, L. Han, J. Xu, M. Liu, L. Zheng, F. P. García de Arquer, C. T. Dinh, F. Fan, M. Yuan, E. Yassitepe, N. Chen, T. Regier, P. Liu, Y. Li, P. De Luna, A. Janmohamed, H. L. Xin, H. Yang, A. Vojvodic, E. H. Sargent, *Science* **2016**, *352*, 333-337.
- [19] a) D. Friebe, M. W. Louie, M. Bajdich, K. E. Sanwald, Y. Cai, A. M. Wise, M. J. Cheng, D. Sokaras, T. C. Weng, R. Alonso-Mori, R. C. Davis, J. R. Bargar, J. K. Norskov, A. Nilsson, A. T. Bell, *J Am Chem Soc* **2015**, *137*, 1305-1313; b) H. Xiao, H. Shin, W. A. Goddard, *Proceedings of the National Academy of Sciences* **2018**, *115*, 5872-5877.
- [20] a) R. Cao, W. Lai, P. Du, *Energy & Environmental Science* **2012**, *5*, 8134-8157; b) T. A. Betley, Q. Wu, T. Van Voorhis, D. G. Nocera, *Inorganic chemistry* **2008**, *47*, 1849-1861.
- [21] a) I. C. Man, H. Y. Su, F. Calle-Vallejo, H. A. Hansen, J. I. Martinez, N. G. Inoglu, J. Kitchin, T. F. Jaramillo, J. K. Norskov, J. Rossmeisl, J. K. Norskov, *Chem Phys* **2005**, *319*, 178-184; c) J. Rossmeisl, Z. W. Qu, H. Zhu, G. J. Kroes, J. K. Norskov, *J Electroanal Chem* **2007**, *607*, 83-89; d) M. Busch, *Current Opinion in Electrochemistry*.
- [22] a) K. P. Jensen, B. O. Roos, U. Ryde, *Journal of Inorganic Biochemistry* **2005**, *99*, 45-54; b) J. R. Winkler, H. B. Gray, in *Molecular Electronic Structures of Transition Metal Complexes I* (Eds.: D. M. P. Mingos, P. Day, J. P. Dahl), Springer Berlin Heidelberg, Berlin, Heidelberg, **2012**, pp. 17-28; c) E. A. Carter, W. A. Goddard, *The Journal of Physical Chemistry* **1988**, *92*, 2109-2115; d) J. M. P. Martinez, E. A. Carter, *J Am Chem Soc* **2019**, *141*, 693-705; e) T. Privalov, L. Sun, B. Akermark, J. Liu, Y. Gao, M. Wang, *Inorg. Chem.* **2007**, *46*, 7075-7086; f) M. Lundberg, M. R. A. Blomberg, P. E. M. Siegbahn, *Inorg. Chem.* **2004**, *43*, 264-274; g) P. E. M. Siegbahn, R. H. Crabtree, *J Am Chem Soc* **1999**, *121*, 117-127.
- [23] M. Busch, A. Fabrizio, S. Luber, J. Hutter, C. Corminboeuf, *J Phys Chem C* **2018**, *122*, 12404-12412.
- [24] J. O. Bockris, T. Otagawa, *J Phys Chem-U.S.* **1983**, *87*, 2960-2971.
- [25] a) M. Busch, N. B. Halck, U. I. Kramm, S. Siahrostami, P. Krtil, J. Rossmeisl, *Nano Energy* **2016**, *29*, 126-135; b) R. Frydendal, M. Busch, N. B. Halck, E. A. Paoli, P. Krtil, I. Chorkendorff, J. Rossmeisl, *Chemcatchem* **2015**, *7*, 149-154.
- [26] N. B. Halck, V. Petrykin, P. Krtil, J. Rossmeisl, *Physical Chemistry Chemical Physics* **2014**, *16*, 13682-13688.
- [27] M. Busch, *Current Opinion in Electrochemistry* **2018**, *9*, 278-284.
- [28] H. Shin, H. Xiao, W. A. Goddard, *J Am Chem Soc* **2018**, *140*, 6745-6748.
- [29] A. D. Doyle, J. H. Montoya, A. Vojvodic, *Chemcatchem* **2015**, *7*, 738-742.
- [30] Z. K. Goldsmith, A. K. Harshan, J. B. Gerken, M. Vörös, G. Galli, S. S. Stahl, S. Hammes-Schiffer, *Proceedings of the National Academy of Sciences* **2017**, *114*, 3050-3055.
- [31] O. Diaz-Morales, I. Ledezma-Yanez, M. T. M. Koper, F. Calle-Vallejo, *ACS Catalysis* **2015**, *5*, 5380-5387.
- [32] M. B. Stevens, L. J. Enman, E. H. Korkus, J. Zaffran, C. D. M. Trang, J. Asbury, M. G. Kast, M. C. Toroker, S. W. Boettcher, *Nano Research* **2019**.
- [33] W. Zhou, L. Guo, *Chemical Society Reviews* **2015**, *44*, 6697-6707.
- [34] S. Zhao, Y. Wang, J. Dong, C.-T. He, H. Yin, P. An, K. Zhao, X. Zhang, C. Gao, L. Zhang, J. Lv, J. Wang, J. Zhang, A. M. Khattak, N. A. Khan, Z. Wei, J. Zhang, S. Liu, H. Zhao, Z. Tang, *Nature Energy* **2016**, *1*, 16184.
- [35] L. Partanen, G. Murdachaew, K. Laasonen, *J Phys Chem C* **2018**, *122*, 12892-12899.
- [36] a) G. Kresse, J. Furthmuller, *Comp Mater Sci* **1996**, *6*, 15-50; b) G. Kresse, J. Furthmuller, *Phys Rev B* **1996**, *54*, 11169-11186.
- [37] C. A. Gaggioli, S. J. Stoneburner, C. J. Cramer, L. Gagliardi, *ACS Catalysis* **2019**, 8481-8502.
- [38] M. Busch, R. B. Wang, A. Hellman, J. Rossmeisl, H. Gronbeck, *J Phys Chem C* **2018**, *122*, 216-226.
- [39] J. Wellendorff, K. T. Lundgaard, A. Møgelhøj, V. Petzold, D. D. Landis, J. K. Norskov, T. Bligaard, K. W. Jacobsen, *Physical Review B* **2012**, *85*, 235149.
- [40] P. E. Blochl, *Phys Rev B* **1994**, *50*, 17953-17979.

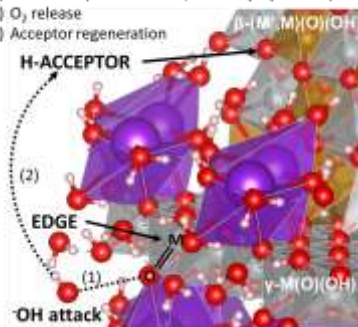
Entry for the Table of Contents (Please choose one layout)

Layout 1:

FULL PAPER

Boosting the oxygen evolution activity
on mixed metal-oxy-hydroxides:
The bifunctional route shows the way

Bifunctional oxygen evolution mechanism
(1) HO – OM bond formation via $\cdot\text{OH}$ attack on edge
(2) H-transfer (H^+ via solvent, e^- via oxy-hydroxide)
(3) O_2 release
(4) Acceptor regeneration



Matthias Vandichel,* Michael Busch,
Kari Laasonen

Page No. – Page No.

Oxygen evolution on metal-oxy-
hydroxides: beneficial role of mixing
Fe, Co, Ni explained via bifunctional
edge/acceptor route way

Layout 2:

FULL PAPER

((Insert TOC Graphic here; max. width: 11.5 cm; max. height: 2.5 cm))

Author(s), Corresponding Author(s)*

Page No. – Page No.

Title

Text for Table of Contents